Electronic Supplementary Material (ESI) for Physical Chemistry Chemical Physics.

Supporting information

for

Surface doping of rubrene single crystals by molecular electron donors and acceptors

Christos Gatsios[1], Andreas Opitz[1,*], Dominique Lungwitz[1], Ahmed E. Mansour[2], Thorsten Schultz[2], Dongguen Shin[1], Sebastian Hammer[3,4], Jens Pflaum[3,5], Yadong Zhang[6], Stephen Barlow[6], Seth R. Marder[6,7] and Norbert Koch[1,2,*]

[1]Institut für Physik & IRIS Adlershof, Humboldt-Universität zu Berlin, 12489 Berlin, Germany

[2]Helmholtz-Zentrum Berlin für Materialien und Energie GmbH, 12489 Berlin, Germany

[3]Experimentelle Physik VI, Julius-Maximilians-Universität Würzburg, 97074 Würzburg, Germany

[4]Center for the Physics of Materials, Departments of Physics and Chemistry, McGill University, Montreal, Qc, Canada

[5]Center for Applied Energy Research e.V., Magdalene-Schoch-Str. 3, 97074 Würzburg, Germany

[6]Renewable and Sustainable Energy Institute (RASEI), University of Colorado Boulder, Boulder, CO 80309, USA

[7]Department of Chemical and Biological Engineering and Department of Chemistry, University of Colorado Boulder, Boulder, CO 80309, USA

*E-Mail: norbert.koch@physik.hu-berlin.de, andreas.opitz@hu-berlin.de

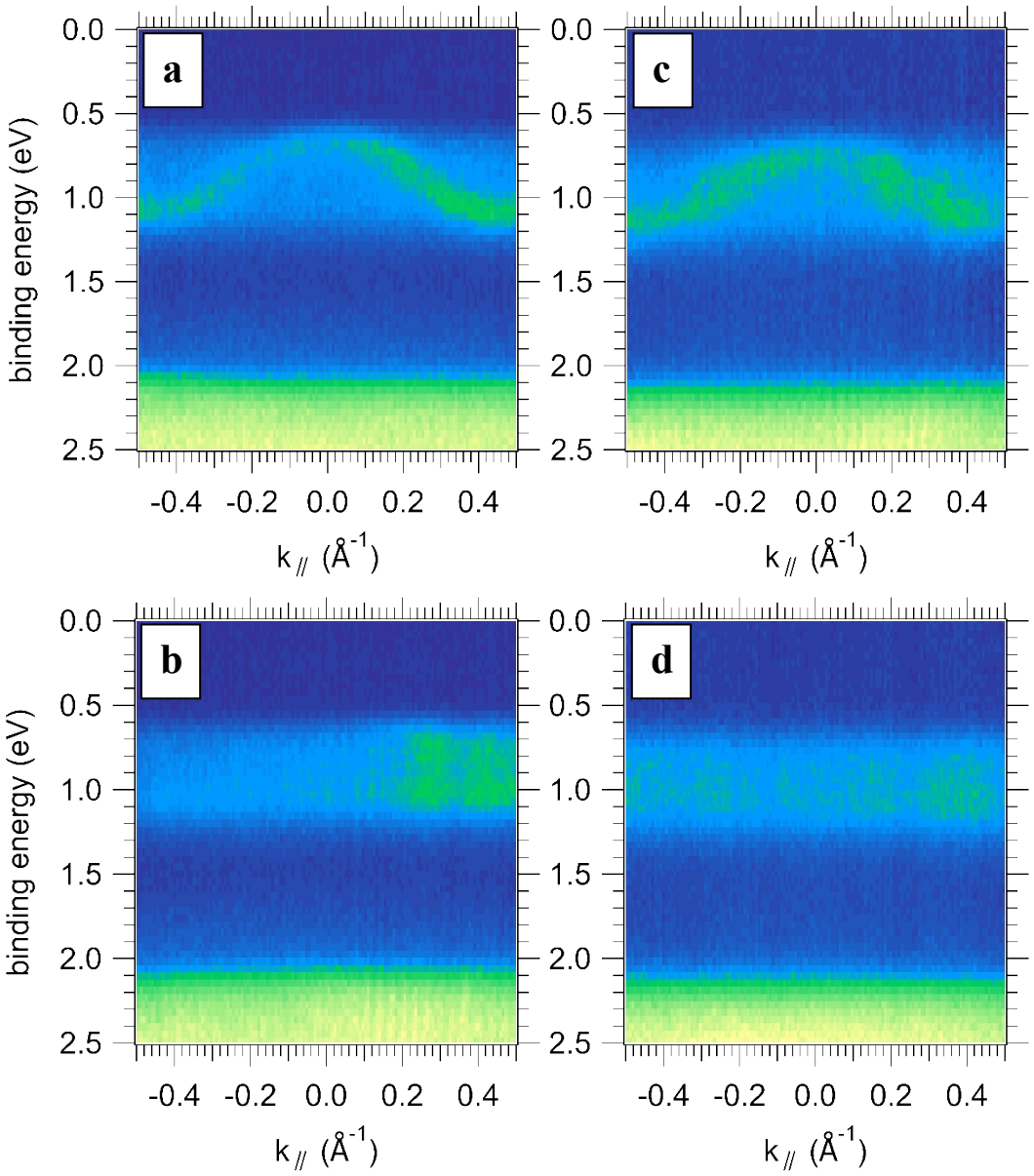

Supplementary Figure S1: 2D spectra of the two bare rubrene single crystal samples measured prior to the surface doping. (a), (b) 2D spectra of the first single crystal rubrene sample along the Γ-Y and Γ-X directions, respectively. (c), (d) 2D spectra of the second single crystal rubrene sample along the Γ-Y and Γ-X directions, respectively. The 2D spectra of the two single crystal rubrene samples show strong qualitative agreement.

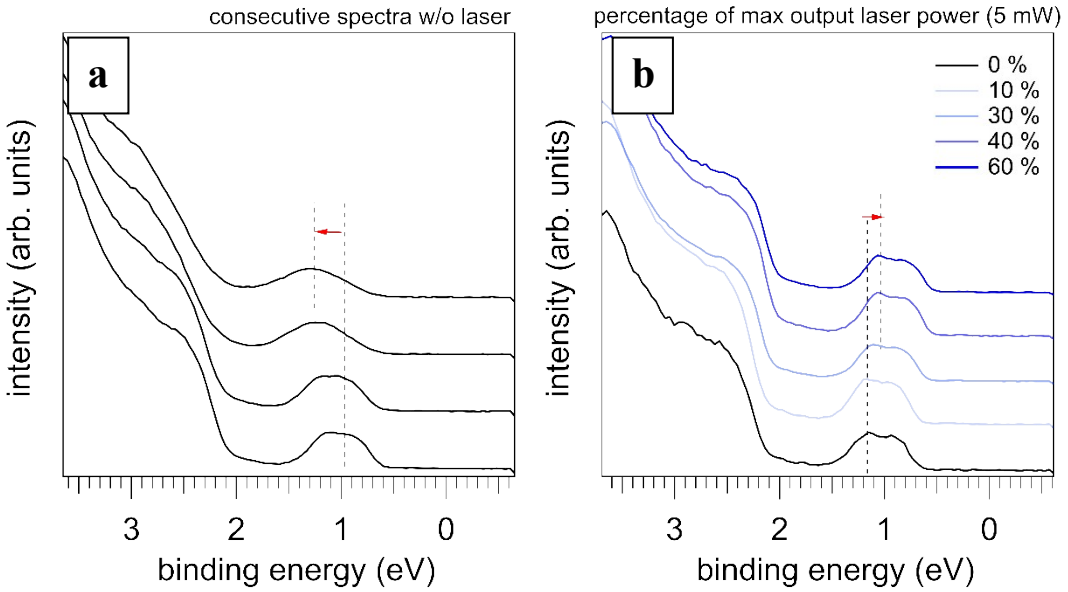

Supplementary Figure S2: Influence of surface charging and its compensation using an external source of light (continuous wave blue laser of 473 nm and with 5 mW max output power). (a) In the absence of laser, consecutive EDCs of equal time durations revealed that the HOMO peak became broader and drifted towards higher binding energies, indicating strong effects of surface charging. By illuminating the sample with a blue laser we could compensate the effect of charging (b). The progressive increase of the laser output power shifts the HOMO peak of rubrene back to lower binding energies. With laser power greater than 40 percent, the position and the shape of the peak stabilized. Given that the diameter of the defocused laser beam is approximately 16 mm, 60 percent of laser power corresponds to a nominal power density of 0.3 mW/cm^2.

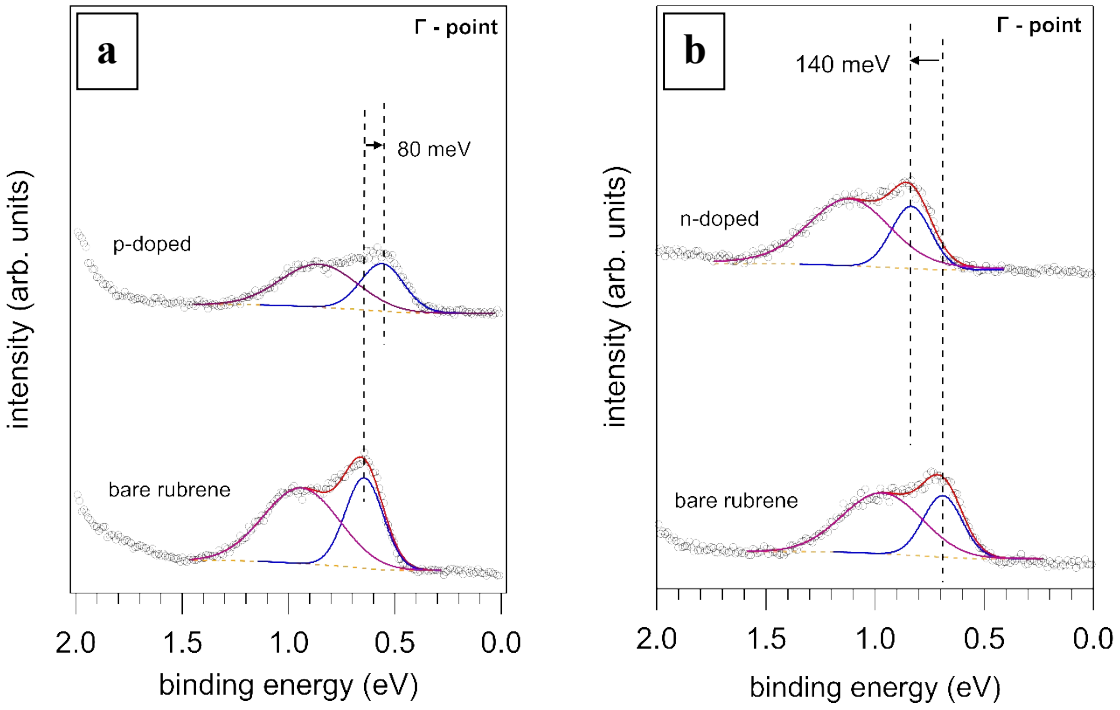

Supplementary Figure S3: Quantitative analysis of the HOMO peak at the Γ point of bare and surface-doped rubrene. The total HOMO peak was deconvoluted using two Voigt functions to account for the dispersive H_1 peak and the satellite feature A. Voigt functions are preferred for fitting photoelectron peaks, as they are convolutions of Gaussian and Lorentzian profiles that represent the instrumental broadening and the natural broadening due to the lifetime of the photoexcited state, respectively. The empty circles indicate the raw data points, the blue Voigt function represents the H_1 peak, whereas the purple is associated to the A satellite peak. The yellow dashed background corresponds to the Shirley background. The red curves represent the total least-squares fitting curve of the valence peak. The black vertical dashed lines depict the positions of the H_1 peaks before and after doping. The fitting parameters are listed in Table S1. For Mo(tfd-CO_2Me)$_3$ (p-doping), the H_1 peak shows a shift of 80 meV towards lower binding energies (a). In the case of $CoCp_2$ (n-doping), the H_1 peak shifts by 140 meV towards higher binding energies (b). The intensity from the HOMO peak of rubrene is attenuated due to the deposition of the molecular dopant layers on the surface.

Supplementary Table S1: Least-square fitting parameters of Figure S4. $\mathbf{E_{H1}}$ is the energy position of the dispersive H_1 peak, $\mathbf{E_A}$ the energy position of the satellite A feature, $\mathbf{FWHM_{H1}}$ and $\mathbf{FWHM_A}$ the full width at half maximum of the peak H_1 and A, respectively.

	$\mathbf{E_{H1}}$ **(eV)**	$\mathbf{FWHM_{H1}}$ **(eV)**	$\mathbf{E_A}$ **(eV)**	$\mathbf{FWHM_A}$ (eV)
bare rubrene	0.64 ± 0.01	0.21 ± 0.04	0.94 ± 0.02	0.42 ± 0.08
p-doped	0.56 ± 0.01	0.24 ± 0.05	0.86 ± 0.02	0.42 ± 0.09
bare rubrene	0.69 ± 0.01	0.21 ± 0.05	0.97 ± 0.02	0.43 ± 0.08
n-doped	0.83 ± 0.01	0.21 ± 0.05	1.12 ± 0.02	0.44 ± 0.08

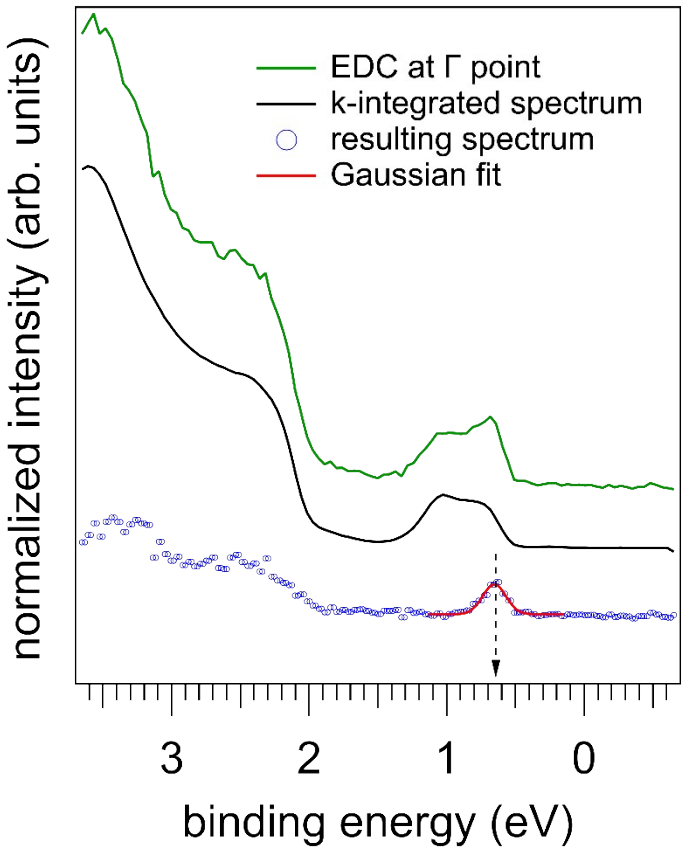

Supplementary Figure S4: Background subtraction procedure applied to the EDC at the Γ point. The exact methodology for subtracting the background from the 2D spectra can be clearly depicted in the figure above. The green curve represents the *k*-resolved EDC, the black curve corresponds to the *k*-integrated spectrum that has been normalized relative to the satellite feature's intensity. The blue dotted line represents the spectrum remaining after subtraction of the k-resolved EDC and the *k*-integrated spectrum. The red line corresponds to the Gaussian fit of the residual spectrum, from which the energy position of the dispersive H_1 peak is determined.

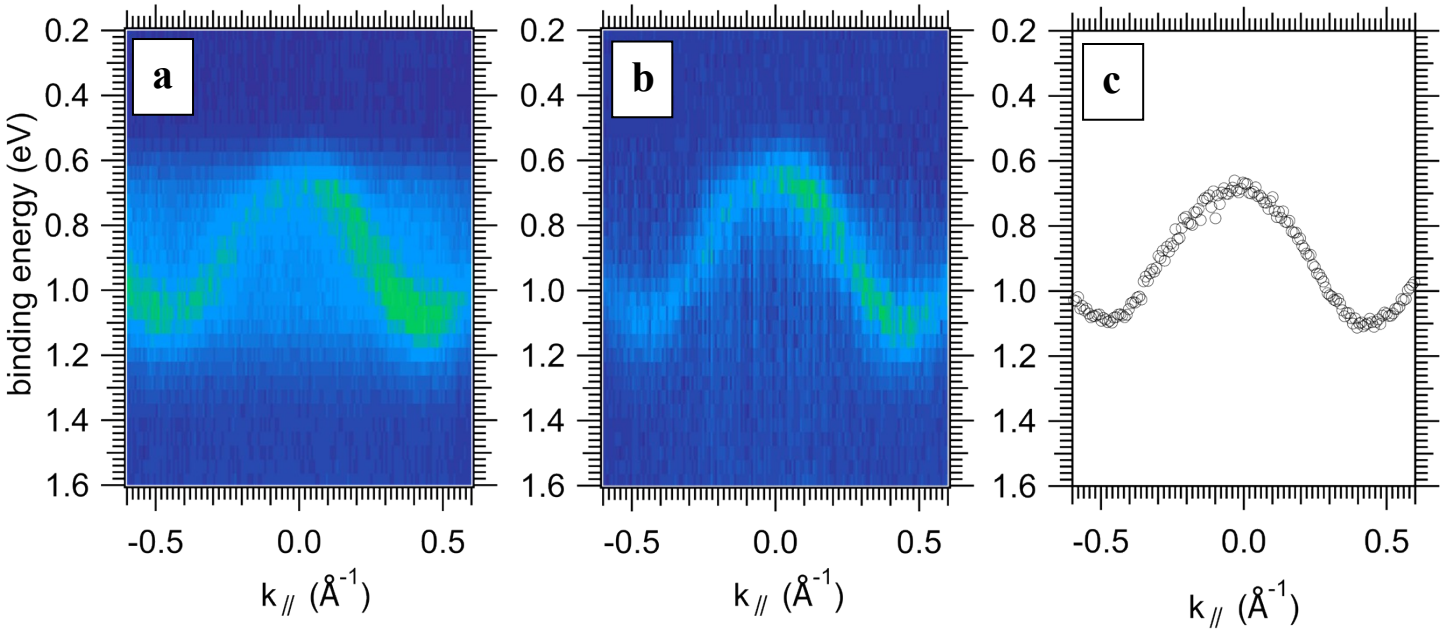

Supplementary Figure S5: Background subtraction applied to the 2D spectra. By using the background subtraction approach illustrated in Figure S5 to all k-resolved EDCs, we were able to eliminate the contribution of the A and B satellites attributed to scattering processes due to the dynamic disorder at room temperature. Specifically, (a) shows the total 2D spectrum of bare rubrene and (b) displays the spectrum remaining after background subtraction. Using a batch fitting script implemented in Igor Pro 9, each residual *k*-resolved profile, was fitted by one Gaussian peak to determine the energy position of the H_1 peak. (c) shows the extracted (E,k) data points corresponding to the H_1 dispersive peak.

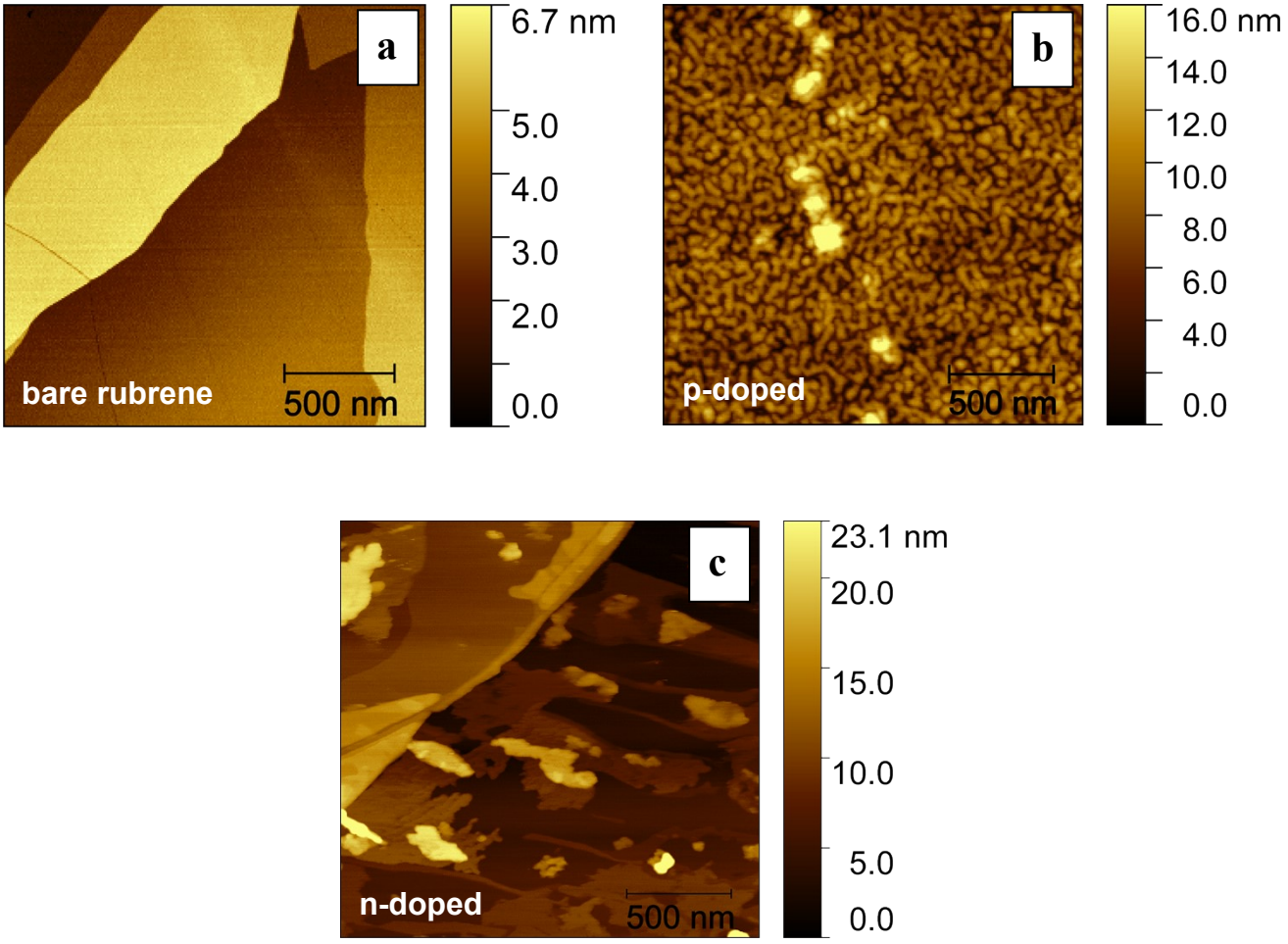

Supplementary Figure S6: Atomic force microscopy (AFM) images. The AFM images depict the surface topography of bare and doped single-crystal rubrene. (a) The bare rubrene reveals a smooth surface characterized by terraces. (b) Upon p-doping with 1.5 nm of the molecular acceptor Mo(tfd-CO2Me)3, a pronounced island growth is evident. (c) The deposition of 4 nm of the n-dopant could be associated with less dense island formations, likely due to the higher volatility of CoCp2.

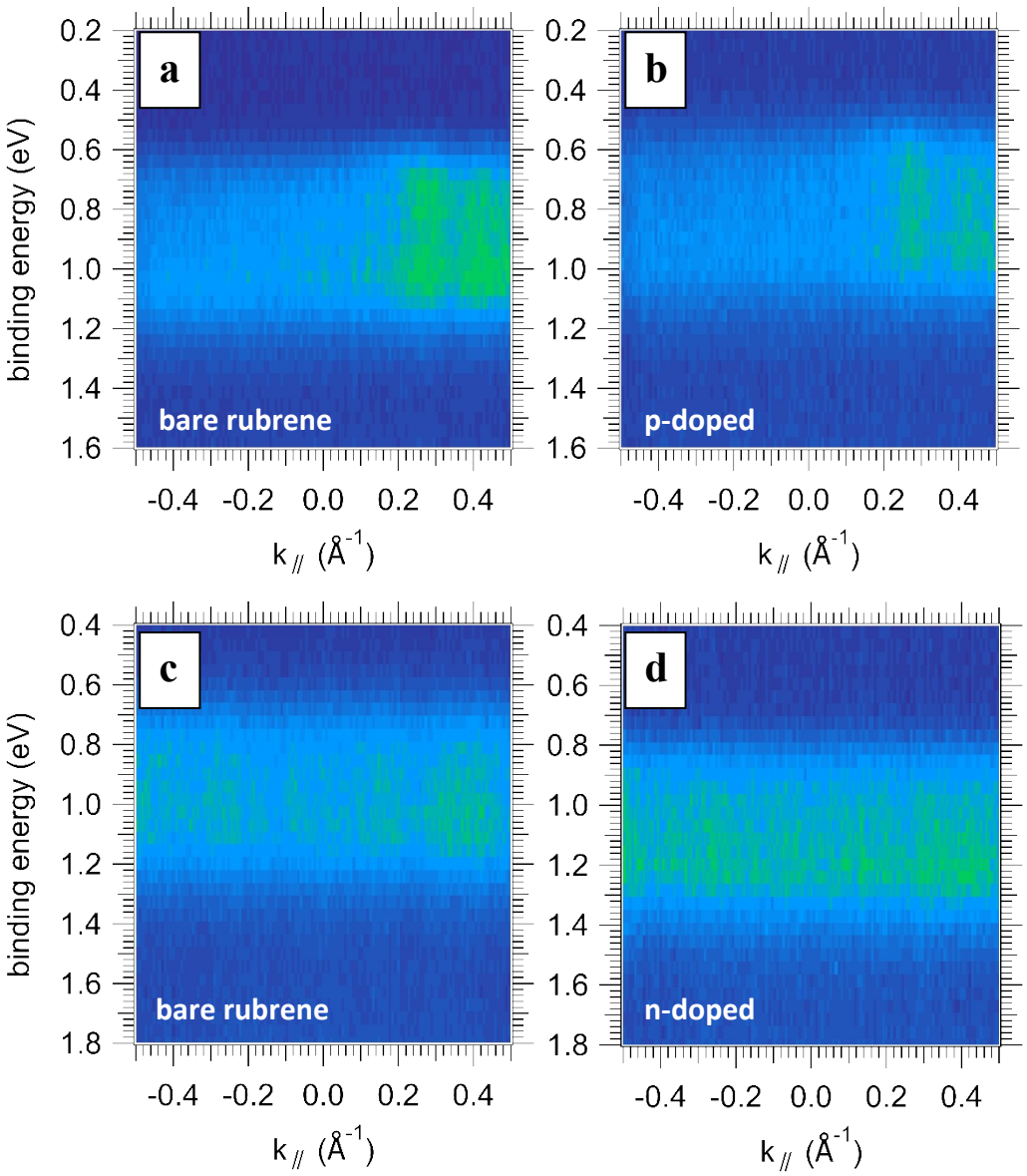

Supplementary Figure S7: Band bending of the valence band of rubrene along the Γ-X directions due to the surface molecular doping. As mentioned in the main text for the case of the valence band along the Γ-Y direction, the charge redistribution at the interface induced by doping results in the bending of all electronic states, including the valence band along the Γ-X direction. In particular, p-doping with Mo(tfd-$CO_2Me)_3$ shifts the valence band towards the Fermi level, (a) to (b). Similarly, when rubrene is n-doped with $CoCp_2$ the valence band shifts away from the Fermi level (c) to (d).

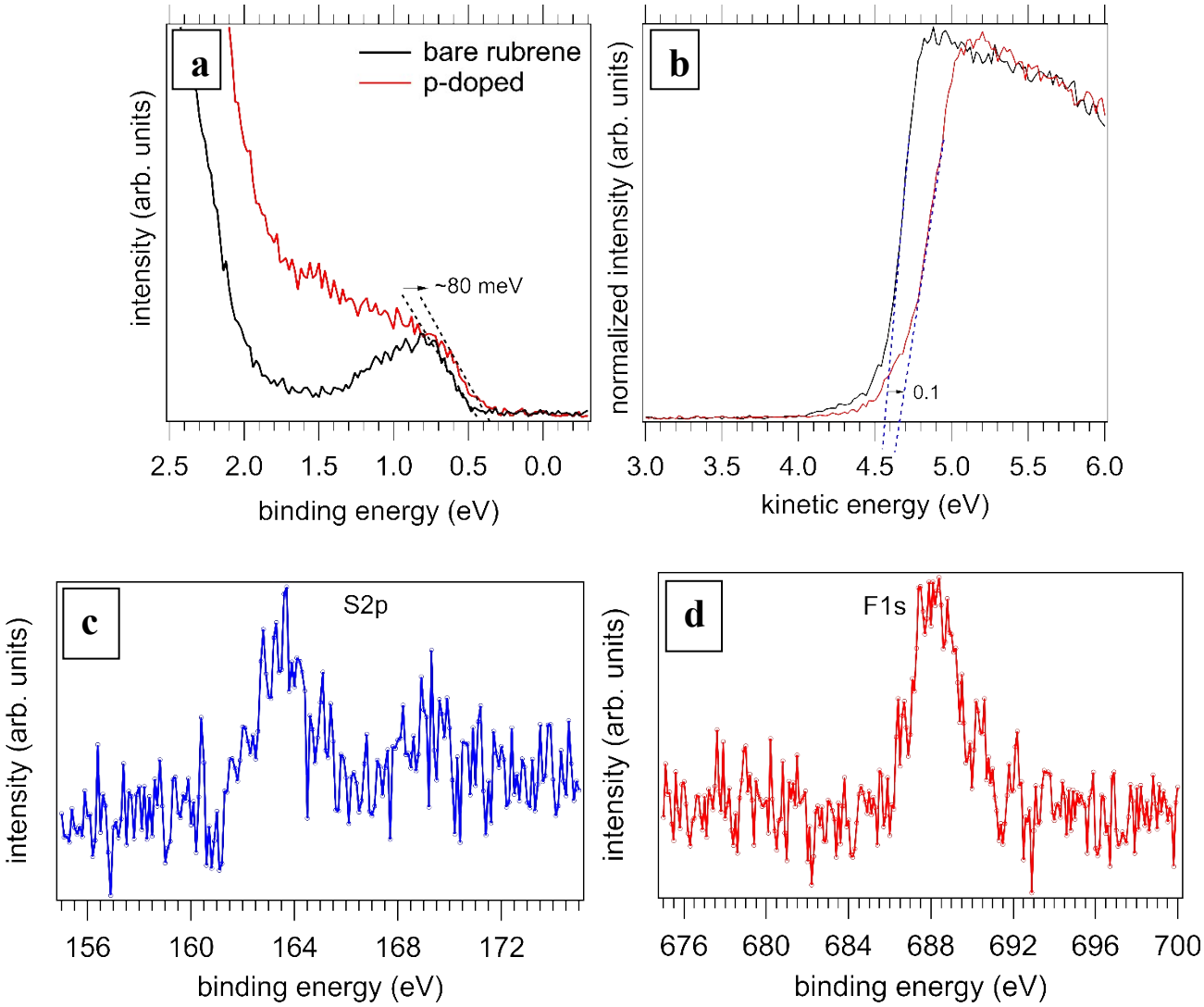

Supplementary Figure S8: Additional ultraviolet (UPS) and X-ray (XPS) photoemission spectra. This figure provides further support to the surface doping of bare rubrene with the molecular acceptor Mo(tfd-$CO_2Me)_3$. Additional UPS and XPS measurements were performed on a standard setup with a He discharge lamp (He-I 21.22 eV) and a hemispherical analyzer (Specs, PHOIBOS 100). The valence region of rubrene (a), was obtained at the Γ point before and after the evaporation of 1.5 nm Mo(tfd-$CO_2Me)_3$. In agreement to what we found in our ArTOF measurements, the evaporation of the dopants induced a shift of the valence peak by approximately 80 meV, as determined by a linear extrapolation of the HOMO peak onsets. After doping the spectrum becomes less structured with the valence peak hidden in the background intensity. This is expected as the dopant adlayer can prevent the electrons from the covered rubrene's surface from being phootemitted. The UPS valence region was recorded with pass energy 10 eV that allows energy resolution of 120 meV. (b) shows the secondary electron cut-off region (SECO). The SECO was obtained using -10 V bias voltage and pass energy 2 eV allowing an energy resolution of 60 meV. The work function can be determined by a linear extrapolation of the onset of the SECO. p-doping increases the work function by roughly 0.1 eV. The shift of the work function is consistent with the band bending of the valence band (80 meV). (c) and (d) show the XPS signals of Sulfur's 2p and Fluorine's 1s core levels, which are present in Mo(tfd-$CO_2Me)_3$.